High-pressure phases of Mg_{2}Si from first principles

Tran Doan Huan, Vu Ngoc Tuoc, Nam Ba Le, Nguyen Viet Minh, and Lilia M. Woods

Phys. Rev. B **93**, 094109 — Published 22 March 2016

DOI: 10.1103/PhysRevB.93.094109

High-pressure phases of magnesium silicide Mg_2Si from first principles

Tran Doan Huan,[1] Vu Ngoc Tuoc,[2] Nam Ba Le,[2,3] Nguyen Viet Minh,[2] and Lilia M. Woods[3,*]

[1] *Department of Materials Science & Engineering and Institute of Materials Science, University of Connecticut, 97 North Eagleville Rd., Unit 3136, Storrs, CT 06269-3136, USA*

[2] *Institute of Engineering Physics, Hanoi University of Science and Technology, 1 Dai Co Viet Rd., Hanoi 10000, Vietnam*

[3] *Department of Physics, University of South Florida, 4202 E. Fowler Ave., Tampa, Florida 33620, USA*

First principles calculations are presented to resolve the possible pressure-dependent phases of Mg_2Si. Although previous reports show that Mg_2Si is characterized by the cubic antiflurite $Fm\bar{3}m$ structure at low pressures, the situation at higher P is less clear with many contradicting results. Here we utilize several methods to examine the stability, electron, phonon, and transport properties of this material as a function of pressure and temperature. We find that Mg_2Si is thermodynamically stable at low and high pressures. Between 6 and 24 GPa, Mg_2Si can transform into Mg_9Si_5, a defected compound, and vice versa, without energy cost. Perhaps this result is related to the aforementioned inconsistency in the structures reported for Mg_2Si within this pressure range. Focusing solely on Mg_2Si, we find a new monoclinic $C2/m$ structure of Mg_2Si, which is stable at high pressures within thermodynamical considerations. The calculated electrical conductivity and Seebeck coefficient taking into account results from the electronic structure calculations help us understand better how transport can be affected in this material by modulating pressure and temperature.

PACS numbers: 77.84.-s 77.65.-j 81.05.Zx

I. INTRODUCTION

Magnesium silicide Mg_2Si is an environmental-friendly material composed of Earth-abundant constituents. These features combined with low-cost production and its attractive properties make Mg_2Si a suitable candidate for different technological applications, including infrared photonic and thermoelectric energy conversion devices. As a narrow-gap semiconductor, Mg_2Si has been envisioned for infrared detectors working in the 1.2 - 1.8 μm wavelength range.[1,2] In addition, Mg_2Si has been considered for thermoelectric applications in the 400-800 K temperature range. The non-toxicity, light weight, and abundance of the comprising elements are advantageous features when compared to other materials, such as PbTe or $CoSb_3$, operating in the same temperature regime. Several reports describe strategies of transport properties optimization via doping for enhanced thermoelectric performance.[3–5] Many computational studies concerning Mg_2Si have been focused on the cubic $Fm\bar{3}m$ (anti-flurite) phase in which this material crystallizes at ambient pressures.[6] Thus further property modifications and addition routes for optimization may become available.

At elevated pressures, available reports for Mg_2Si structures are largely inconsistent. According to the clearest pathway, Mg_2Si transforms from the cubic $Fm\bar{3}m$ to the orthorhombic $Pnma$ (anti-cotunnite) structure[6] at pressure $P \simeq 7$ GPa, followed by a transition to the hexagonal $P6_3/mmc$ (Ni_2In-type) structure at $P \simeq 20$ GPa.[7–9] This pathway does not include some (unresolved) hexagonal structures experimentally observed by Cannon *et al.*[10] and Peun *et al.*[11] Mg_2Si was also found[12] to transfrom from $Fm\bar{3}m$ to an unknown monoclinic phase at $P \simeq 11$ GPa. This new structural phase, which has also not been resolved, was reported[12] to remain stable up to $P \simeq 37$ GPa. Subsequently, the electrical resistivity ρ of Mg_2Si was measured, showing at least three discontinuous pressure points at 7 GPa, 12.2 GPa, and 22.2 GPa.[13] It was suggested[13] that the $Fm\bar{3}m \rightarrow Pnma$ transition occurs between the first two points, i.e., within the range from 7 to 12.2 GPa, while the last point (22.2 GPa) marks the $Pnma \rightarrow P6_3/mmc$ transition. In a more recent experimental work,[14] no structural transition could be detected for pure Mg_2Si under the quasi-hydrostatic pressure up to 15 GPa. However, the $Fm\bar{3}m \rightarrow Pnma$ transition was indeed obsedved[14] on Al-doped Mg_2Si at 11.9 GPa. Other binary phases with different Mg:Si ratio, e.g., Mg_9Si_5 and Mg_5Si_6, may also contribute to this complicated scenario. These materials can be synthesized by precipitation from supersaturated solid solution of Al-Mg-Si alloys.[15–19] In particular, two phases of this solution, i.e., the β' and β'' phases, have been resolved and believed to correspond to the hexagonal $P6_3/m$ phase of Mg_9Si_5[16,20] and monoclinic $C2/m$ phase of Mg_5Si_6,[18,19] respectively.

This contribution aims to explore this unclear picture by first principles simulations. We start by searching for thermodynamically stable configurations of Mg_2Si at zero and various finite P. The stability of the predicted structures with respect to the $P6_3/m$ phase of Mg_9Si_5 and the $C2/m$ phase of Mg_5Si_6 is then assessed via the convex hulls contructed from the enthalpy calculated at different pressures. We find that between 6GPa and 24 GPa, Mg_9Si_5 and Mg_2Si are nearly equivalent in terms of the thermodynamic stability. This result may provide an explanation for the contradicting reports in the literature. Focusing solely on Mg_2Si, we calculated the Gibbs free energy of the predicted structures. We identify two new monoclinic phases of Mg_2Si which belong to the $P2_1$

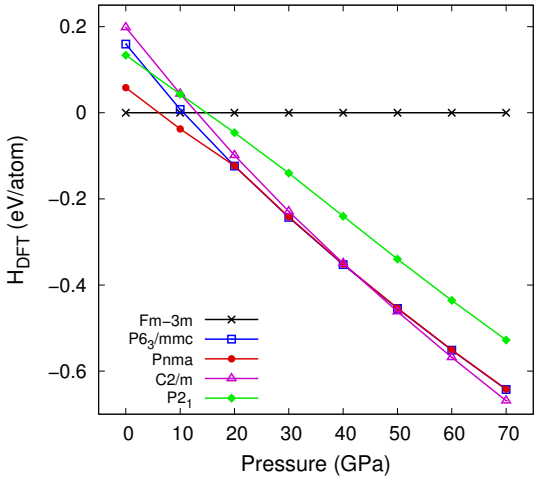

FIG. 1. (Color online) DFT enthalpies $H_{\rm DFT}$ of predicted thermodynamically stable low-energy structures of Mg_2Si. Calculated data is given by symbols while curves are shown as a guide for the eyes.

and the $C2/m$ space groups. Of them, the former might be relevant to the one observed at $P = 16.1$ GPa[12], while the latter is predicted to be a high-pressure Mg_2Si phase at $P \simeq 38$ GPa and above. These pressure-induced transitions are also evaluated using free energy calculations via the lattice dynamics in terms of phonon dispersion spectra. Transport properties, such as the electrical conductivity and Seebeck coefficient, are calculated within the Boltzmann's transport theory and discussed in terms of the structural changes induced by the pressure.

II. COMPUTATIONAL METHODS

To investigate the pressure-induced transitions and the properties of the stable phases, we employ several computational methods. First principles calculations reported herein were performed within the density functional theory (DFT)[21,22] formalism as implemented in the *Vienna Ab-initio Simulation Package* (VASP),[23–26] using the semi-local Perdew-Burke-Ernzerhof exchange-correlation energy functional.[27] Highly accurate DFT total energies, $E_{\rm DFT}$, were ensured by a Monkhorst-Pack **k**-point mesh[28] of no less than $9 \times 9 \times 9$ sampling of the Brilouin zone, and a basis set of plane waves with kinetic energy cutoff of 500 eV for expanding the wavefunctions. Both, the cell and atomic degrees of freedom of the examined structures, were optimized under different hydrostatic compressive pressures until the residual forces were obtained to be below 10^{-2} eV/Å. In addition to the standard DFT simulations with the PBE semi-local XC functional, electronic structure calculations are also performed utilizing the hybrid Heyd-Scuseria-Ernzerhof (HSE06) functional.[29,30] PBE calculations typically underestimate the values for the energy gaps,[31] however the HSE functional is believed to give more accurate results thanks to the better description of the localized states forming the bonds. More specifically, a part of the semi-local exchange energy is replaced by that from the exact non-local Fock exchange, which results in bringing the calculated HSE06 band gap closer to its true value.

Low-enthalpy structures of compressed crystalline matter can be efficiently predicted at finite pressures by many searching methods at the DFT level.[32–36] Herein, we used the minima-hopping approach[37–39] to search for possible stable Mg_2Si structures at hydrostatic pressures up to 70 GPa. This method, which relies on extensively exploring the DFT energy landscape of a given chemical composition, has successfully been used for various classes of crystalline materials[34,40–42] The phonon frequency spectra and related vibrational free energies for each system are examined within the supercell approach as implemented in the PHONOPY package.[43,44] Calculations of the transport properties, such as the electrical conductivity and Seebeck coefficient for the various structures, are carried utilizing the constant relaxation time τ approximation as implemented in the BoltzTrap code.[45] Taking constant τ in general is a good approximation as long as its energy changes are ate a smaller scale as compared to the energy changes in the density of states, which is typically the case for metals and many semiconductors.[46,47] Thus the primary effects captured using these computational methods are due to the underlying electronic structure as a function of pressure.

III. THERMODYNAMICALLY STABLE STRUCTURES

A. Mg-Si binaries

In addition to the known $Fm\bar{3}m$, $Pnma$, and $P6_3/mmc$ structures, our search for low-enthalpy structures of Mg_2Si returns two new monoclinic phases, namely $C2/m$ and $P2_1$. All phases are examined by calculating the enthalpy $H = E_{\rm DFT} + PV$, where $E_{\rm DFT}$ is the DFT energy and V is the simulation cell volume (the zero-point energy correction is not included). The results are displayed in Fig. 1 showing that the thermodynamic stability for the known phases at finite pressures agrees well with the ones reported by experimental and previous theoretical works.[6–9] In particular, the pressure-driven transitions of Mg_2Si are $Fm\bar{3}m \rightarrow Pnma \rightarrow P6_3/mmc$ with two critical points at 8 GPa and 20 GPa. These two transitions are consistent with the two out of the three transitions observed experimentally[13] (the third one was suggested[13] to be related to the mixture of $Fm\bar{3}m$ and $Pnma$). In addition, we found that the monoclinic $C2/m$ structure becomes thermodynamically most stable at $P \geq 38$ GPa. Results from the phonon spectra calculations also clearly indicate that all of these structures are dynamically stable (the phonon band structures are given in Fig. 1 in the Supplementary Material together

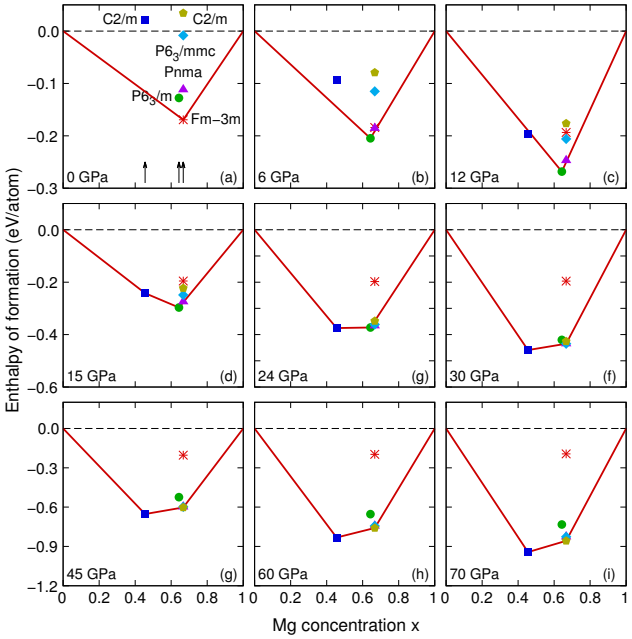

FIG. 2. (Color online) DFT enthalpies of formation $\Delta H_{\rm DFT}$ of the examined structrures of Mg-Si binary compounds, given by symbols and labeled by the space group name, computed at different pressure P. In (a), three vertical arrows are placed at $x = 0.455$, $x = 0.643$, and $x = 0.667$ to indicate Mg_5Si_6, Mg_9Si_5, and Mg_2Si, respectively. Red lines are used to construct the convex hulls of the most stable phases of Mg-Si binaries with different Mg concentration x.

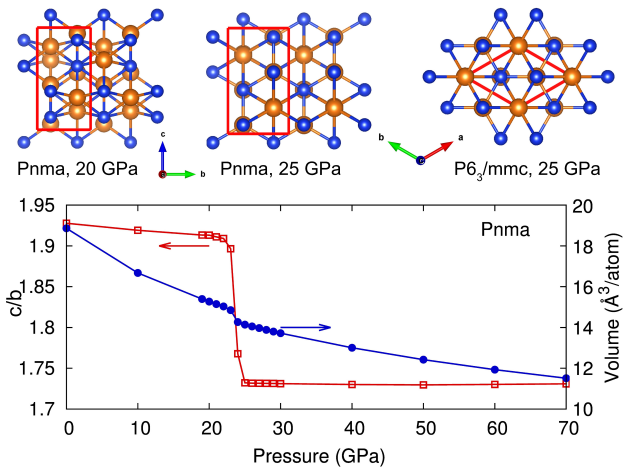

FIG. 3. (Color online) (Top panel) Top views of the $Pnma$ and the $P6_3/mmc$ structure of Mg_2Si at 20 and 25 GPa. (Bottom panel) c/b ratio (red squares) and volume per atom (blue circles) of the $Pmna$ structure as functions of pressure P. On the top row, the unit cells of the orthorhombic $Pnma$ and hexagonal $P6_3/mmc$ structures are shown as red rectangles and diamond, respectively.

with their crystallographic information in Table 1).

We consider the stability of Mg_2Si with respect to Mg_9Si_5 and Mg_5Si_6, the precipitated Mg-Si binary compounds observed in the solid solution of Al-Mg-Si alloys.[15,16,18–20] The proposed structure of Mg_9Si_5 is $P6_3/m$, which was found[16] to be about 50meV/atom lower than the $P6_3/mmc$ phase of Mg_2Si by first-principles calculations. For Mg_5Si_6, the resolved structure is $C2/m$.[18,19] For this goal, we computed the enthalpy of formation $\Delta H_{\rm DFT}$ of all the known structures of Mg_5Si_6, Mg_9Si_5, and Mg_2Si using the following experession

$$\Delta H_{\rm DFT} = H(\mathrm{Mg}_x\mathrm{Si}_{1-x}) - [xH(\mathrm{Mg}) + (1-x)H(\mathrm{Si})]. \quad (1)$$

Here, $H(\mathrm{Mg}_x\mathrm{Si}_{1-x})$ is the enthalpy of the Mg-Si binary with Mg concentration x while $H(\mathrm{Mg})$ and $H(\mathrm{Si})$ are the calculated enthalpies of the hexagonal $P6_3/mmc$ crystal of Mg and the cubic $Fd\bar{3}m$ crystal of Si. The enthalpy of formation $\Delta H_{\rm DFT}$ calculated at different pressure P is shown in Fig. 2.

Consistent with a previous report,[16] we found that at $P = 0$GPa, the $P6_3/m$ structure of Mg_9Si_5 is about 100 meV/atom lower than the $P6_3/mmc$ structure of Mg_2Si. This structure is also lower than the $Pnma$ structure of Mg_2Si by about 15 meV/atom while it is higher than the $Fm\bar{3}m$ structure. Therefore, Mg_2Si is stable at the cubic $Fm\bar{3}m$ phase while both Mg_9Si_5 and Mg_5Si_6 are metastable. This conclusion is also consistent with another work[48] of the Mg-Si binaries based on first-principles calculations. When the pressure is elevated, the $Pnma$, $P6_3/mmc$, and $C2/m$ structures of Mg_2Si become increasingly more stable. Between 6 and 24 GPa, the $Pnma$ phase of Mg_2Si lies on the straight line connecting Mg_9Si_5 and pure Mg ($x = 1$), clearly implying that Mg_2Si and Mg_9Si_5 can transform from one to the other without energy cost. Perhaps this interesting scenario provides an explanation for the fact that a variety of different structures, i.e., orthorhombic $Pnma$[7–9], hexagonal,[10,11] and monoclinic,[12] have been reported for Mg_2Si at medium pressures.

Within the next two pressure regimes, i.e., from 24−38 GPa and above 38 GPa, we find that the $P6_3/mmc$ and $C2/m$ structures of Mg_2Si, respectively, are thermodynamically stable. Moreover, starting from 12 GPa, the $C2/m$ structure of Mg_5Si_6 becomes stable with respect to the decomposition into pure Si and Mg_9Si_5, and this binary can also be formed, as observed experimentally.[18,19]

B. Magnesium silicide Mg_2Si

We now focus on the possible structures of Mg_2Si only. The results in Fig. 1 also demonstrate that under external hydrostatic pressure, the $Pnma$ structure gradually distorts and then directly transforms to the $P6_3/mmc$ structure at the critical point of $P_c \simeq 24$ GPa. This situation is further elucidated in Fig. 3 by showing the c/b ratio as a function of pressure. One finds that before

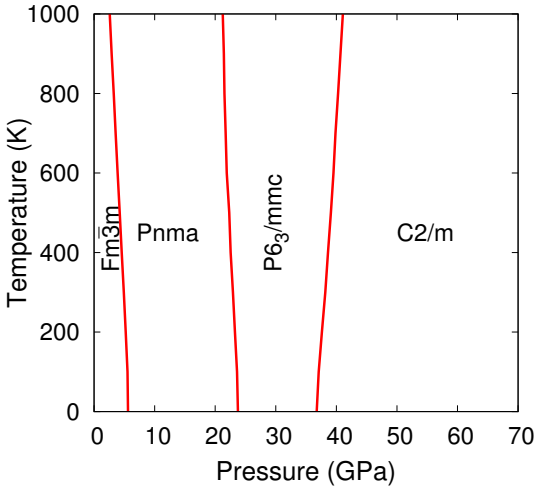

FIG. 4. (Color online) Temperature-pressure phase diagram of Mg_2Si constructed from the Gibbs free energies.

the critical point the c/b ratio of the $Pmna$ structure is roughly 1.92. After passing the P_c point, a is reduced from 6.12 Å to 5.42 Å and b undergoes a discontinuous expansion from 3.96 Å to 4.23 Å, bringing the c/b ratio down to $\sqrt{3} \simeq 1.73$. In this transition process, the volume V is changed by about 1% and the atomic positions of the $Pnma$ lattice become slightly rearranged, recovering the hexagonal $P6_3/mmc$ structure. For an illustration, the top views of the $Pmna$ structure below and above P_c together with the top view of the $P6_3/mmc$ structure are shown as well. The identical atomic arrangement at $P = 25$ GPa is additionally confirmed by the simulated x-ray diffraction patterns provided in Fig. 2 of the Supplementary Material.[49]

Fig. 1 also confirms that $Pmna$ and $P6_3/mmc$ are stable between 8 and 45 GPa, implying that the unknown monoclinic phase observed by Zhu *et al.*[12] between 11 and 37 GPa is metastable. While the atomic positions of this observed structure have yet to be resolved experimentally,[12] the cell parameters were determined to be $a = 7.965$ Å, $b = 7.720$ Å, $c = 6.704$ Å, and $\beta = 112.5°$ at $P = 16.1$ GPa.[12] The cell parameters for the predicted monoclinic $P2_1$ structure are somewhat similar, i.e., $a = 7.833$ Å, $b = 7.812$ Å, $c = 6.782$ Å, and $\beta = 115.4°$. However, due to experimental uncertainties it is not clear if the simulated x-ray diffraction pattern of the $P2_1$ structure agrees completely with the reported measurements (see Fig. 3 of the Supplementary Material[49] for more information). Therefore, further experimental work is needed to resolve this metastable phase.

The examined thermodynamic stability of Mg_2Si via the enthalpy $H_{\rm DFT}$ is applicable at $T = 0$ K. In order to include temperature effects into the analysis, we estimate the Gibbs free energy $G(P,T) = H_{\rm DFT} + F_{\rm vib}(T)$, where the vibrational free energy $F_{\rm vib}(T)$ is calculated within the harmonic approximation from the phonon density of states $g(\omega)$ as

$$F_{\rm vib}(T) = rk_{\rm B}T \int_0^\infty d\omega g(\omega) \ln\left[2\sinh\left(\frac{\hbar\omega}{2k_{\rm B}T}\right)\right]. \quad (2)$$

Here, r is the number of degrees of freedom in the unit cell, $k_{\rm B}$ the Boltzmann's constant, and $\hbar$ the reduced Planck's constant. We note that the zero-point energy correction, which was neglected in Fig. 1, is included in $G(P,T)$ and the phonon density of states are consistent with the phonon dispersion spectra, given in the Supplementary Material. For many crystalline materials, this approach gives reasonable predictions for the temperature dependent thermodynamic stability,[34,35] which makes it an attractive tool for this study.

The temperature-pressure phase diagram is constructed from the Gibbs energy $G(P,T)$. The obtained results are displayed in Fig. 4 showing that up to 1000 K and 70 GPa, Mg_2Si adopts four structural phases. From low to high pressures, the stable phases are $Fm\bar{3}m$, $Pnma$, $P6_3/mmc$, and $C2/m$. The phase transition points between them are estimated to be $\simeq 6$ GPa, $\simeq 24$ GPa, and $\simeq 38$ GPa, respectively, depending weakly on temperature. In addition, no temperature-driven phase transition is predicted below 1000 K.

IV. ELECTRONIC PROPERTIES

Mg_2Si at ambient pressure can be characterized as a narrow band gap semiconductor with $E_g \simeq 0.7$ eV[50] before transforming into a metallic solid at elevated pressures.[13] Attempts to experimentally determine the behavior of E_g as a function of P were conducted, but no conclusive results were obtained.[51] In particular, it was suggested that the pressure coefficient $(\partial E_g/\partial P)_{T=300\rm K}$ of the Mg_2Si band gap at room temperature is within the accuracy error of the measurements $\pm 0.5 \times 10^{-2}$eV/GPa leaving the general trend of E_g vs. P unclear.

Here we calculate the band gap of the $Fm\bar{3}m$ phase as a function of P and the results are shown in Fig. 5. It is found that indirect $E_g = 0.16$ eV with PBE while by using HSE06, we obtained a considerably higher value of $E_g = 0.57$ eV at $P = 0$. Note that the energy gap obtained via HSE06 calculations is very close to the experimentally observed indirect $E_g = 0.69$ eV at $T = 4$ K[1] as well as the calculated value of 0.65 eV at the GW level of DFT.[52] By linearly fitting the calculated data, we found that with PBE, $(\partial E_g/\partial P)_{T=0\rm K} = -1.80 \times 10^{-2}$ eV/GPa while with HSE06, this coefficient is $(\partial E_g/\partial P)_{T=0\rm K} = -1.64 \times 10^{-2}$ eV/GPa. Thus increasing P results in a linear-like decrease of the gap at a slightly lower HSE06 rate as compared to the PBE one. We note that this value was calculated at 0K, and that at the room temperature, $(\partial E_g/\partial P)$ may be closer to that given in Ref. 51.

The Mg_2Si properties are also examined by considering the calculated electronic band structure for the different stable phases. In Fig. 6 the band structures of

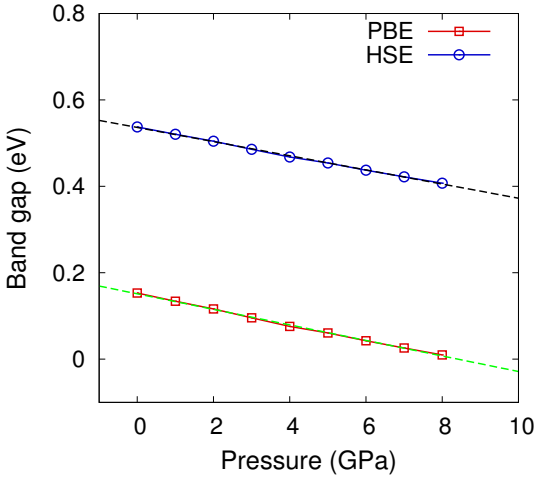

FIG. 5. (Color online) Band gap of the $Fm\bar{3}m$ phase calculated at various pressure using the PBE and HSE06 XC functionals. Calculated data is shown by symbols while dotted lines show the linear fits to this data.

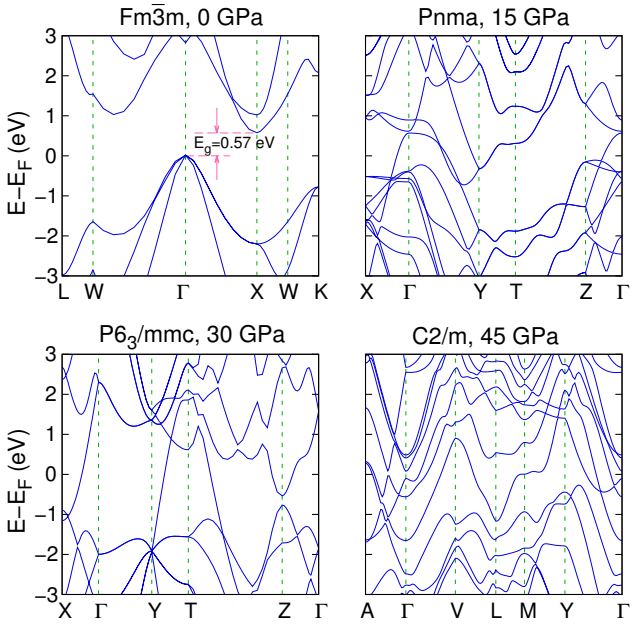

FIG. 6. (Color online) Energy band structures calculated at the HSE06 level for four phases of Mg_2Si at their stable pressure: $Fm\bar{3}m$ at 0 GPa, $Pnma$ at 15 GPa, $P6_3/mmc$ at 30 GPa, and $C2/m$ at 45 GPa. The indirect band gap $E_g = 0.57$ eV of the $Fm\bar{3}m$ phase is indicated in the top left panel of the figure.

the $Fm\bar{3}m$, $Pnma$, $P6_3/mmc$, and $C2/m$ phases at 0, 15, 30, and 45 GPa, respectively, are shown. The corresponding densities of states are provided in Fig. 4 of the Supplementary Material.[49] Fig. 6 demonstrates that the $Fm\bar{3}m$ is a semiconductor with an indirect band gap while the other phases are metallic. For the newly predicted phase, namely $C2/m$, the valence bands near the Fermi energy are dominated by the Si-3p states while the conduction bands near the Fermi energy are composed of comparable Si-3s, Si-3p, Mg-2p, and Mg-3s contributions (see Fig. 4 of the Supplementary Material).

V. TRANSPORT PROPERTIES

The electronic structure is directly related to the transport characteristics, such as electrical conductivity (σ) and Seebeck coefficient (S), of a given material. These transport properties are of primary importance for limiting the thermoelectric transport. Reported measurements at room temperature[13] show that in the range of 0 GPa to 25 GPa the electrical resistivity $\rho = 1/\sigma$ of Mg_2Si displays four distinguishable regimes and three of them can be assigned to known phases, namely $Fm\bar{3}m$, $Pnma$, and $P6_3/mmc$, while the fourth corresponds to a mixture of the $Pnma$ and $P6_3/mmc$ phases.

Here we utilize Boltzmann's theory as implemented in the BoltzTraP code to gain insight into the transport of Mg_2Si under pressure by calculating σ and S for the various phases.[45] The BoltzTraP code is considered a state of the art computational approach to investigate transport properties in crystals.[53,54] In fact, it has recently been used to study σ and S of the $Fm\bar{3}m$ phase of Mg_2Si considering the effects of strain and doping.[54] The reported BoltzTraP simulations for the $Fm\bar{3}m$, $Pnma$, and $P6_3/mmc$ structures include a number of band structure calculations with very dense **k**-points meshes. In particular, we used a mesh of $45\times45\times45$ for the $Fm\bar{3}m$, a mesh of $25\times41\times22$ for the $Pnma$, a mesh of $45\times45\times45$ for the $P6_3/mmc$, and a mesh of $21\times21\times21$ for the $C2/m$ structures. Using these results, σ/τ (τ is the relaxation scattering time) is computed. Because the HSE06 treatment is prohibitively expensive for these meshes, PBE was used for the calculations. We expect that with this numerical prescription, general trends of the calculated transport properties are captured.

The calculated conductivity normalized to σ_{300K} at $P = 0$ is shown in Fig. 7 (a). One finds that the computational results previously reported for the $Fm\bar{3}m$ at $P = 0$ GPa[54] are accurately reproduced. Fig. 7 shows that at any given temperature (300K, 400K, or 500K), σ of this phase is enhanced by almost an order of magnitude as P increases to 6 GPa (such an increase is also consistent with recent experiments[13]). This behavior can be explained by the reduction of the semiconducting energy gap of the $Fm\bar{3}m$ phase as the pressure is increased, which is demonstrated in Sec. IV. The $Fm\bar{3}m \rightarrow Pnma$ and the $Pnma \rightarrow P6_3/mmc$ transitions occurring at $P \sim 6$ GPa and $P \sim 24$ GPa lead to the discontinuity of σ vs P with the magnitude of roughly one order. The $P6_3/mmc$ to $C2/m$ transition, however, does not change σ significantly. Fig. 7 also shows that σ is rather weakly dependent on temperature and pressure for all metallic phases.

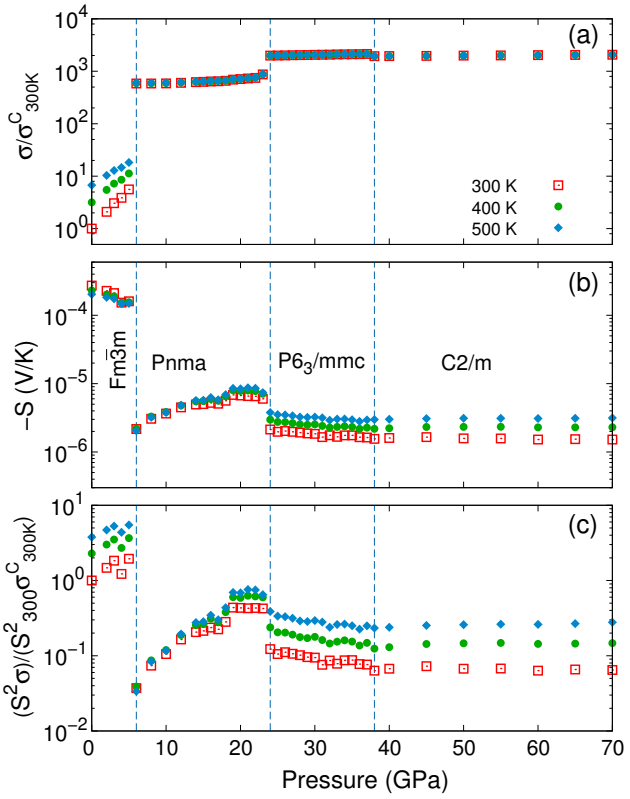

FIG. 7. (Color online) (a) Electrical conductivity σ of the thermodynamically stable phases of Mg_2Si up to 70 GPa normalized to σ^{C}_{300K}, which corresponds to the conductivity of the cubic $Fm\bar{3}m$ phase at $P = 0$ GPa and $T = 300$K. (b) The magnitude of the corresponding Seebeck coefficient $-S$ and (c) The dimensionless power factor $(S^2\sigma)/(S^2_{300}\sigma^{C}_{300})$ as a function of P. S_{300} denotes the Seebeck coefficient of the cubic phase at $P = 0$ GPa and $T = 300$K. Vertical dashed lines indicate the theoretically determined phase transition points (6 GPa for $Fm\bar{3}m \rightarrow Pnma$, 24 GPa for $Pnma \rightarrow P6_3/mmc$, and 38 GPa for $P6_3/mmc \rightarrow C2/m$).

The calculated Seebeck coefficient S of Mg_2Si is reported in Fig. 7 (b). At $T = 300$ K and $P = 0$ GPa, we obtained $S = -2.71 \times 10^{-4}$V/K, which is consistent with recent measurements[55] and calculations.[54] As P is raised, the magnitude of S decreases in a linear-like fashion, which is consistent with the reduction of E_g of the $Fm\bar{3}m$ phase. At the transition point of $P = 6$ GPa, the Seebeck coefficient drops down by more than an order of magnitude followed by a linear (temperature-independent) increase in P. Besides the discontinuity at $P = 20$ GPa marking the transition to the $P6_3/mmc$ phases, $-S$ is fairly insensitive to the pressure. For the last phase, the Seebeck coefficient shows a behavior vs. P consistent with the one of a material becoming a stronger metal. The temperature dependence of the $C2/m$ structure is also much more pronounced as compared to the other structures.

The results for the calculated transport properties are useful in obtaining a better understanding of the thermoelectric behavior of Mg_2Si. The performance of a thermoelectric device is determined by the dimensionless figure of merit $ZT = S^2\sigma T/\kappa$ (κ - thermal conductivity) as larger ZT warrants a more effective device.[3–5] Here we find that the power factor $S^2\sigma$ of Mg_2Si can experience significant enhancement as pressure and temperature are elevated. Our results in Fig. 7(c) show that the scaled power factor is largest at $P \lesssim 6$ GPa and $T = 500$ K. This correlates with the much enhanced conductivity and relatively large Seebeck coefficient due to the reduction of the energy band gap as the material approaches the first structural phase transition (Fig. 7(a,b)). We also find that the power factor exhibits a maximum at $P \sim 22$ GPa, however its magnitude is much smaller than the one around 6 GPa. Thus our calculations indicate that the best charge carrier thermoelectric properties can be achieved at higher temperatures and elevated pressure before the structural transition to $Pnma$ takes place.

VI. SUMMARY

In summary, we have studied the possible structural phases of Mg_2Si over wide ranges of pressure ($0-70$ GPa) and temperature ($0-1000$ K) using first-principles simulations. While Mg_2Si is found to be stable at low and high pressure, it is nearly equivalent with Mg_9Si_5 from 6 to 24 GPa. We suggest that this finding may offer an explanation for the current inconsistency in the reported structures of Mg_2Si within this pressure range. Thermodynamical considerations based on Gibbs free energy calculations reveal that this material has a new monoclinic phase ($C2/m$), which become stable at $P \geq 38$ GPa. We show that the sequence of finite pressure Mg_2Si phases is $Fm\bar{3}m \rightarrow Pnma \rightarrow P6_3/mmc \rightarrow C2/m$ with transition points at $\simeq 6$ GPa, $\simeq 24$ GPa, and $\simeq 38$ GPa, which appear to be weakly dependent on temperature. Electronic structure and phonon dispersion spectra are also obtained and used to examine the structural features, stability and electron and phonon properties. Calculations utilizing the Boltzmann transport theory take into account the electronic structure properties for estimating the electrical conductivity and Seebeck coefficient in terms of pressure and temperature. While our first-principles calculations are in agreement with reported work on some of the known Mg_2Si phases, novel results in terms of electronic, phonon, and transport properties for a wide pressure and temperature ranges may be useful for further fundamental and technological exploration of this material. Our finidngs provide not only a comprehensive understanding of the properties of the various Mg_2Si phases as a function of temperature and pressure, but they can also serve as useful guidelines for experimentalists when searching for the optimum thermoelectric performance range of this environmentally safe material.

ACKNOWLEDGMENTS

The authors thank S. Goedecker and M. Amsler for the minima-hopping code, and P. Boulet and F. Zhu for valuable discussions. They also thank two anonimous reviewers for useful comments that have enabled significant improvements of the manuscript. Work by V.N.T. is supported by the Vietnam National Foundation for Science and Technology Development under Grant 103.01-2014.25. L.M.W. acknowledges support from the US National Science Foundation under Grant No. DMR-1400957. Part of the computational work (by T.D.H.) was made possible through the XSEDE computational resource allocation number TG-DMR150033. L.M.W and N.B.L. also acknowledge the use of the University of South Florida Research Computing facilities.

* lmwoods@usf.edu

[1] H. Udono, H. Tajima, M. Uchikoshi, and M. Itakura, Jpn. J. Appl. Phys. **54**, 07JB06 (2015).
[2] H. Udono, Y. Yamanaka, M. Uchikoshi, and M. Itakura, J. Phys. Chem. Solids **74**, 311 (2013).
[3] V. K. Zaitsev, M. I. Fedorov, E. A. Gurieva, I. S. Eremin, P. P. Konstantinov, A. Y. Samunin, and M. V. Vedernikov, Phys. Rev. B **74**, 045207 (2006).
[4] W. Liu, X. Tan, K. Yin, H. Liu, X. Tang, J. Shi, Q. Zhang, and C. Uher, Phys. Rev. Lett. **108**, 166601 (2012).
[5] N. V. Morozova, S. V. Ovsyannikov, I. V. Korobeinikov, A. E. Karkin, K. Takarabe, Y. Mori, S. Nakamura, and V. V. Shchennikov, J. Appl. Phys. **115**, 213705 (2014).
[6] E. Y. Tonkov, *High Pressure Phase Transformations: A Handbook* (Gordan and Breach Science, Philadelphia, US, 1992).
[7] J. Hao, B. Zou, P. Zhu, C. Gao, Y. Li, D. Liu, K. Wang, W. Lei, Q. Cui, and G. Zou, Solid State Commun. **149**, 689 (2009).
[8] J.-H. Hao, Z.-G. Guo, and Q.-H. Jin, Solid State Commun. **150**, 2299 (2010).
[9] F. Yu, J.-X. Sun, W. Yang, R.-G. Tian, and G.-F. Ji, Solid State Commun. **150**, 620 (2010).
[10] P. Cannon and E. T. Conlin, Science **145**, 487 (1964).
[11] T. Peun, J. Lauterjung, and E. Hinze, Nucl. Instr. Meth. Phys. Res. B **97**, 483 (1995).
[12] F. Zhu, X. Wu, S. Qin, and J. Liu, Solid State Commun. **152**, 2160 (2012).
[13] W. Ren, Y. Han, C. Liu, N. Su, Y. Li, B. Ma, Y. Ma, and C. Gao, Solid State Commun. **152**, 440 (2012).
[14] J. Zhao, Z. Liu, R. A. Gordon, K. Takarabe, J. Reid, and J. S. Tse, J. Appl. Phys. **118**, (2015).
[15] M. A. van Huis, J. H. Chen, H. W. Zandbergen, and M. H. F. Sluiter, Acta Mater. **54**, 2945 (2006).
[16] R. Vissers, M. A. van Huis, J. Jansen, H. W. Zandbergen, C. D. Marioara, and S. J. Andersen, Acta Mater. **55**, 3815 (2007).
[17] S. Ji, M. Tanaka, S. Zhang, and S. Yamanaka, Inorg. Chem. **51**, 10300 (2012).
[18] H. W. Zandbergen, S. J. Andersen, and J. Jansen, Science **277**, 1221 (1997).
[19] S. J. Andersen, H. W. Zandbergen, J. Jansen, C. Traeholt, U. Tundal, and O. Reiso, Acta Mater. **46**, 3283 (1998).
[20] C. Ravi and C. Wolverton, Acta Mater. **52**, 4213 (2004).
[21] P. Hohenberg and W. Kohn, Phys. Rev. **136**, B864 (1964).
[22] W. Kohn and L. Sham, Phys. Rev. **140**, A1133 (1965).
[23] G. Kresse and J. Hafner, Phys. Rev. B **47**, 558 (1993).
[24] G. Kresse, Ph.D. thesis, Technische Universität Wien, 1993.
[25] G. Kresse and J. Furthmüller, Comput. Mater. Sci. **6**, 15 (1996).
[26] G. Kresse and J. Furthmüller, Phys. Rev. B **54**, 11169 (1996).
[27] J. P. Perdew, K. Burke, and M. Ernzerhof, Phys. Rev. Lett. **77**, 3865 (1996).
[28] H. J. Monkhorst and J. D. Pack, Phys. Rev. B **13**, 5188 (1976).
[29] J. Heyd, G. E. Scuseria, and M. Ernzerhof, J. Chem. Phys. **118**, 8207 (2003).
[30] J. Heyd, G. E. Scuseria, and M. Ernzerhof, J. Chem. Phys. **124**, 219906 (2006).
[31] J. P. Perdew, Int. J. Quant. Chem. **28**, 497 (1985).
[32] Y. Wang and Y. Ma, J. Chem. Phys. **140**, 040901 (2014).
[33] E. Zurek and W. Grochala, Phys. Chem. Chem. Phys. **17**, 2917 (2015).
[34] T. D. Huan, V. Sharma, G. A. Rossetti, and R. Ramprasad, Phys. Rev. B **90**, 064111 (2014).
[35] H. Sharma, V. Sharma, and T. D. Huan, Phys. Chem. Chem. Phys. **17**, 18146 (2015).
[36] C. Fan and J. Li, Phys. Chem. Chem. Phys. **17**, 12970 (2015).
[37] S. Goedecker, J. Chem. Phys. **120**, 9911 (2004).
[38] M. Amsler and S. Goedecker, J. Chem. Phys. **133**, 224104 (2010).
[39] S. Goedecker, in *Modern Methods of Crystal Structure Prediction*, edited by A. R. Oganov (Wiley-VCH, Weinheim, Germany, 2011), Chap. 7, pp. 147–180.
[40] T. D. Huan, M. Amsler, V. N. Tuoc, A. Willand, and S. Goedecker, Phys. Rev. B **86**, 224110 (2012).
[41] T. D. Huan, M. Amsler, R. Sabatini, V. N. Tuoc, N. B. Le, L. M. Woods, N. Marzari, and S. Goedecker, Phys. Rev. B **88**, 024108 (2013).
[42] T. D. Huan, M. Amsler, M. A. L. Marques, S. Botti, A. Willand, and S. Goedecker, Phys. Rev. Lett. **110**, 135502 (2013).
[43] A. Togo, F. Oba, and I. Tanaka, Phys. Rev. B **78**, 134106 (2008).
[44] K. Parlinski, Z-. Q. Li, and Y. Kawazoe, Phys. Rev. Lett. **78**, 4063 (1997).
[45] G. K. Madsen and D. J. Singh, Comput. Phys. Commun. **175**, 67 (2006).
[46] D. Parker and D. J. Singh, Phys. Rev. B **82**, 035204 (2010).
[47] D. J. Singh, Phys. Rev. B **76**, 085110 (2007).
[48] I. Opahle, G. K. H. Madsen, and R. Drautz, Phys. Chem. Chem. Phys. **14**, 16197 (2012).
[49] See Supplemental Material for more information reported in this paper.
[50] D. M. Rowe, *CRC Handbook of Thermoelectrics* (CRC Press, USA, 1995).
[51] A. Stella, A. D. Brothers, R. H. Hopkins, and D. W. Lynch, Phys. Stat. Solidi (b) **23**, 697 (1967).

[52] B. Arnaud and M. Alouani, Phys. Rev. B **64**, 033202 (2001).
[53] R. Chmielowski, D. Péré, C. Bera, I. Opahle, W. Xie, S. Jacob, F. Capet, P. Roussel, A. Weidenkaff, G. K. H. Madsen, and G. Dennler, J. Appl. Phys. **117**, 125103 (2015).
[54] H. Balout, P. Boulet, and M.-C. Record, J. Electron. Mater. **43**, 3801 (2014).
[55] H. J. Lee, Y. R. Cho, and I.-H. Kim, J. Ceramic Proc. Research **12**, 16 (2011).